GDCh
Research Articles
Angewandte Chemie
International Edition
www.angewandte.org

How to cite: *Angew. Chem. Int. Ed.* **2023**, e202307395
doi.org/10.1002/anie.202307395

Solar Cells | Hot Paper

Managing Excess Lead Iodide with Functionalized Oxo-Graphene Nanosheets for Stable Perovskite Solar Cells

Guixiang Li[+], *Yalei Hu*[+], *Meng Li,* Ying Tang, Zuhong Zhang, Artem Musiienko, Qing Cao, Fatima Akhundova, Jinzhao Li, Karunanantharajah Prashanthan, Fengjiu Yang, Patryk Janasik, Augustine N. S. Appiah, Sergei Trofimov, Nikolaos Livakas, Shengnan Zuo, Luyan Wu, Luyao Wang, Yuqian Yang, Benjamin Agyei-Tuffour, Rowan W. MacQueen, Boris Naydenov, Thomas Unold, Eva Unger, Ece Aktas,* Siegfried Eigler,* and Antonio Abate**

Abstract: Stability issues could prevent lead halide perovskite solar cells (PSCs) from commercialization despite it having a comparable power conversion efficiency (PCE) to silicon solar cells. Overcoming drawbacks affecting their long-term stability is gaining incremental importance. Excess lead iodide (PbI_2) causes perovskite degradation, although it aids in crystal growth and defect passivation. Herein, we synthesized functionalized oxo-graphene nanosheets (Dec-oxoG NSs) to effectively manage the excess PbI_2. Dec-oxoG NSs provide anchoring sites to bind the excess PbI_2 and passivate perovskite grain boundaries, thereby reducing charge recombination loss and significantly boosting the extraction of free electrons. The inclusion of Dec-oxoG NSs leads to a PCE of 23.7 % in inverted (p-i-n) PSCs. The devices retain 93.8 % of their initial efficiency after 1,000 hours of tracking at maximum power points under continuous one-sun illumination and exhibit high stability under thermal and ambient conditions.

---

[*] Dr. G. Li,[+] Prof. Dr. M. Li, Y. Tang, Z. Zhang
Key Lab for Special Functional Materials of Ministry of Education, National & Local Joint Engineering Research Center for High-efficiency Display and Lighting Technology, School of Materials Science and Engineering, Collaborative Innovation Center of Nano Functional Materials and Applications, Henan University
Kaifeng 475004 (China)
E-mail: mengli@henu.edu.cn

Dr. G. Li,[+] Prof. Dr. M. Li, Dr. A. Musiienko, F. Akhundova, J. Li, K. Prashanthan, Dr. F. Yang, S. Trofimov, S. Zuo, L. Wu, L. Wang, Dr. Y. Yang, Dr. B. Agyei-Tuffour, Dr. R. W. MacQueen, Dr. B. Naydenov, Dr. T. Unold, Prof. Dr. E. Unger, Prof. Dr. A. Abate
Helmholtz-Zentrum Berlin für Materialien und Energie GmbH
Hahn-Meitner-Platz 1, 14109 Berlin (Germany)
E-mail: antonio.abate@helmholtz-berlin.de

Dr. G. Li,[+] Prof. Dr. A. Abate
Department of Chemistry, Bielefeld University
Universitätsstraße 25, 33615 Bielefeld (Germany)

Dr. G. Li[+]
Present address: Institute of Chemical Sciences and Engineering, École Polytechnique Fédérale de Lausanne (EPFL)
1015 Lausanne (Switzerland)

Dr. Y. Hu,[+] Q. Cao, Prof. Dr. S. Eigler
Institute of Chemistry and Biochemistry, Freie Universität Berlin
Altensteinstraße 23a, 14195 Berlin (Germany)
E-mail: siegfried.eigler@fu-berlin.de

Dr. Y. Hu[+]
CNRS, Immunology, Immunopathology and Therapeutic Chemistry, UPR3572, University of Strasbourg, ISIS
67000 Strasbourg (France)

K. Prashanthan
Department of Physics, University of Jaffna
Jaffna 40000 (Sri Lanka)

P. Janasik, A. N. S. Appiah
Silesian University of Technology
44-100 Gliwice (Poland)

N. Livakas
Nanochemistry Department, Istituto Italiano di Tecnologia
Via Morego 30, 16163 Genova (Italy)
and
Department of Chemistry and Industrial Chemistry, Universitàdegli Studi di Genova
Via Dodecaneso 31, 16146 Genova (Italy)

L. Wu
Department of Physics, Università di Cagliari
Cittadella Universitaria, 09042 Monserrato (Italy)

Dr. B. Agyei-Tuffour
Department of Materials Science and Engineering, School of Engineering Sciences, College of Basic and Applied Sciences, University of Ghana
Legon, GA-521-1966 Accra (Ghana)

Dr. E. Aktas, Prof. Dr. A. Abate
Department of Chemical, Materials and Production Engineering, University of Naples Federico II. Naples
pzz.le Vincenzo Tecchio 80, 80125 Naples (Italy)
E-mail: ece.aktas@unina.it

[+] These authors contributed equally to this work.

Introduction

Lead halide perovskite solar cells (PSCs) have received widespread attention as a promising contender in emerging photovoltaics (PVs). During the past decade, the PSCs have achieved incredibly rapid progress in power conversion efficiency (PCE) from 3.8 % to 25.7 %.[1] What stands out in PSCs is the brilliant optoelectronic properties of perovskites, for instance, ultrahigh absorption coefficient,[2] tunable band gaps,[3] superior defect tolerance,[4] and long carrier diffusion length,[5] as well as low manufacturing costs.[6] Notwithstanding having remarkable optoelectronic properties and surpassing the efficiency of silicon solar cells, the lack of long-term stability is one of the main roadblocks towards its industrialization.[7] In 2016, Saliba et al. reported that to use a multi-cation and anion composited perovskite absorber layer can be an alternative solution for their long-term stability issue.[8] Since then, cesium ion (Cs^+) has been incorporated in the perovskite composition to achieve more reproducible devices with high PCE and long-term stability.[9] In principle, adding more inorganic elements into the perovskite precursor increases mixing entropy and replaces volatile organic cations that can generally improve the stability of devices.[10]

However, undesirable excess halide phases within the perovskite film will eventually lead to irreversible long-term stability issues.[11] Likewise, as reported in the previous studies, the light-induced phase segregation process can be observed while exposing the multiple halide-based perovskite device to constant illumination.[12] Nevertheless, using excess lead iodide (PbI_2) in perovskite precursor ensures larger grain, reduces halide vacancies, and promotes oriented α-phase perovskite crystal growth.[13] Additionally, excess or residual PbI_2 plays a role in passivating grain boundary defects.[13a,14] Nonetheless, PbI_2 is readily decomposed into metallic lead (Pb^0) by releasing iodine (I_2) vapor under continuous light illumination and heating. These species generate nonradiative recombination centers and promote ion migration, thereby accelerating the attenuation of the device performance due to chemical chain reactions.[15] Consequently, stabilizing excess PbI_2 is essential to improve the long-term operational stability of PSCs.

Graphene derivatives have been utilized as two-dimensional (2D) network structural materials in solar cells due to having high electrical conductivity, chemical stability, and superior semiconductor properties.[16] Lin et al. successfully employed graphene on both sides of Cu–Ni alloy electrodes in PSCs to stabilize the electrodes by suppressing light- and heat-induced component migration.[17] In our previous work, dodecylamine-based ultrathin 2D graphene network was used to control ion migration in triple-cation perovskites against external environmental factors.[18] However, no work has completely stabilized excess PbI_2 via 2D (graphene) network materials, which still limits the operational stability of PSCs.

In this work, we modified the functionalization of graphene nanosheets for managing excess PbI_2 in perovskites, resulting in more efficient and stable devices. Specifically, we prepared functionalized oxo-graphene nanosheets (Dec-oxoG NSs) using hydroxyl radicals prepared via wet-chemical etching. We show that Dec-oxoG NSs stabilize excess PbI_2 release during the crystallization of perovskite films. PSCs prepared with Dec-oxoG NSs showed significantly better charge extraction enabling a champion power conversion efficiency of 23.7 % in p-i-n architecture. The Dec-oxoG-based device retained 93.8 % of its initial PCE after 1,000 h tracking at maximum power points (MPP) under continuous one sun illumination, as well as high stabilities under 85 °C test and ambient conditions.

Results and Discussion

Tailoring material functionalization

Oxo-graphene nanosheets (oxoG NSs) were prepared using wet chemical synthesis.[19] Hereafter, we prepared functionalized oxoG NSs (Dec-oxoG NSs) by etching oxoG with hydroxyl radicals ($HO^\bullet$), which were generated by the photolysis of hydrogen peroxide with UV light under the catalysis of Fe^{2+} (Figure 1a).[20] During this process, $HO^\bullet$ oxidizes the hydroxyl groups to carbonyl groups and carboxylic acids by attacking the unsaturated aromatic ring and phenol-like groups of oxoG via electrophilic addition and oxidation reactions.[20]

The morphological properties of oxoG and as-prepared Dec-oxoG NSs were presented by atomic force microscope (AFM). As expected, the pristine oxoG NSs were flat, and no pores were observed (Figure 1b). After etching, the surface of Dec-oxoG NSs became rough, and some pores appeared across the Dec-oxoG NSs surface (Figures 1c and S1, ESI†). From AFM images, we can also observe the thin-layer structure of Dec-oxoG NSs. Raman spectroscopy was then used to give more information about the structural characteristics. As shown in Figure 1d, the intensity ratio of disordered/defect-activated D band and graphitized G bands (I_D/I_G) was increased from 1.15 for oxoG NSs to 1.18 for Dec-oxoG NSs. Associated with that the broad full width at half maximum (FWHM) of the 2D peak ($>100\ cm^{-1}$), we can learn Dec-oxoG NSs retaining a high functionalization degree. Fourier transform infrared spectroscopy (FTIR) spectra were utilized to study the functional groups, observing stretching vibrations of O–H at about 3330 cm^{-1}, stretching vibrations of C=O at around 1720 cm^{-1}, deformation vibrations of the O–H at about 1405 cm^{-1}, and stretching vibrations of C–O at around 1155 cm^{-1} for both oxoG and Dec-oxoG (Figure S2, ESI†).[21] To further investigate the chemical composition of oxoG and Dec-oxoG NSs, X-ray photoelectron spectroscopy (XPS) and solid-state nuclear magnetic resonance (ssNMR) spectra were performed. As shown in Figure 1e, the high-resolution C 1s spectrum showed typical features for oxoG with the peaks assigned to C–C, C–OH/C–O–C, and C=O/COOH bonds. The proportion of higher oxidised atoms (11.0 %) in Dec-oxoG NSs, such as carbonyl or carboxyl, was more than that (5.3 %) in oxoG NSs. Also, the ratio of C=O/COOH to C–O–C/C–OH increased from 0.13 to 0.39 after etching. In the ssNMR spectra of oxoG and Dec-oxoG NSs (Figure S3,

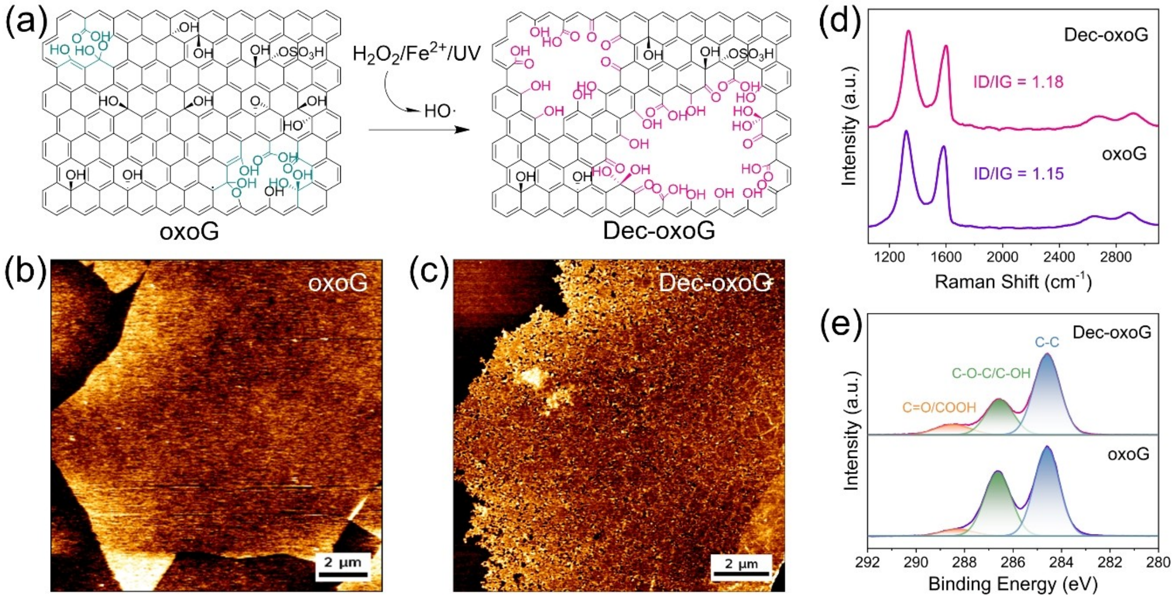

Figure 1. (a) Reaction schematic for the conversion of functional groups in the basal plane of oxoG. AFM images of (b) oxoG and (c) Dec-oxoG NSs. (d) Average Raman spectra, (e) high-resolution C1s XPS spectra for oxoG and Dec-oxoG NSs.

ESI[†]), the signal of graphitic sp^2 atoms, tertiary alcohols and epoxides were found, and the ratio of tertiary alcohols to epoxides increased from 0.17 to 0.64 after etching.[22] These results indicated that the proportion of oxo-groups like hydroxyl, carbonyl, and carboxyl groups at the rims of generated pores increased for Dec-oxoG NSs.

Origins of enhancing crystal structure

After demonstrating the functionalized structure of the Dec-oxoG NSs, we investigated its interaction with perovskite using FTIR spectra. The FTIR study confirms the presence of Dec-oxoG in the perovskite film and reveals their interaction. The green curve in Figure 2a labelled "Pure Dec-oxoG" represents freshly prepared Dec-oxoG NSs without perovskite layer. The pink curve's "Dec-oxoG"

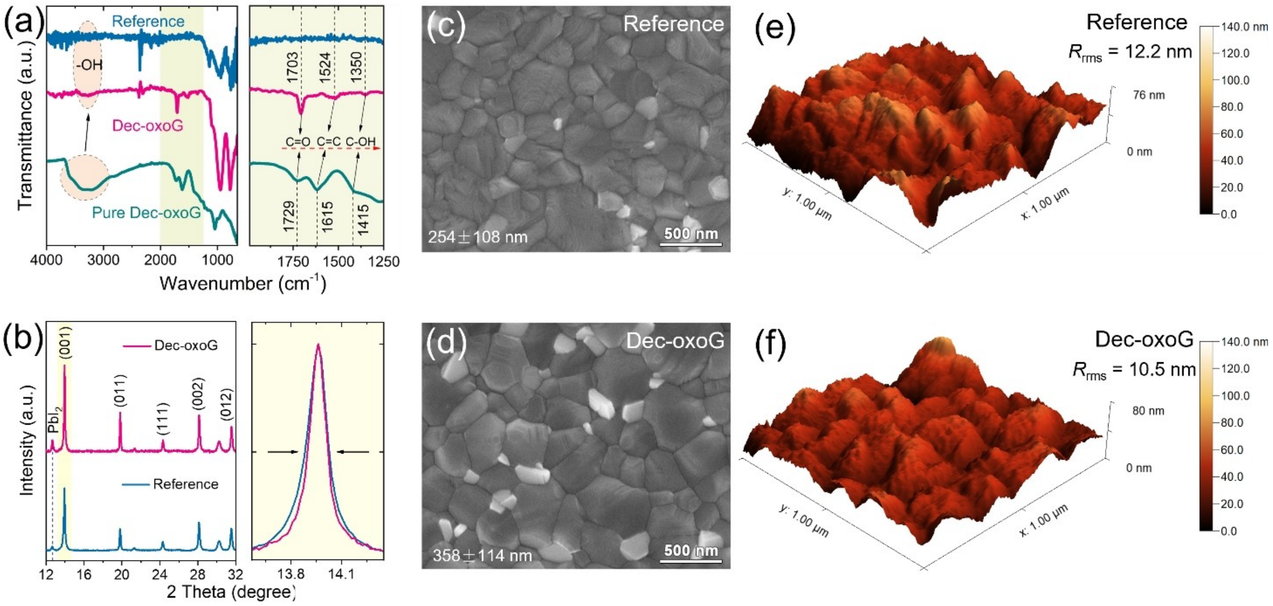

Figure 2. (a) FTIR spectra, (b) XRD patterns of the reference and Dec-oxoG NSs perovskite films. Top-view SEM images of the (c) reference film and (d) film optimized with Dec-oxoG. 3D AFM images of the surface morphologies of (e) reference and (f) Dec-oxoG perovskite films.

depicts the perovskite film treated with Dec-oxoG NSs, and "Reference" marked by the dark blue curve represents pristine perovskite sample without Dec-oxoG NSs (see the method section in Supporting Information for details). We noticed that the stretching vibration of ν(O–H) in pure Dec-oxoG NSs appeared at $\approx$3300 cm^{-1}, while it slightly presents in Dec-oxoG NSs treated perovskite film and is not visible in Reference film (Figure 2a). The typical peaks of ν(C=O), ν(C=C) and ν(C–OH) vibrations in pure Dec-oxoG NSs are observed at 1729 cm^{-1}, 1615 cm^{-1}, and 1415 cm^{-1}, respectively. We note that the stretching vibration of the double bond has shifted due to having lower bond strength between sulphur and oxygen due to the adduct formation.[23] Likewise, these peak shifts to the lower wavenumber of 1703 cm^{-1} for ν(C=O), 1524 cm^{-1} for ν(C=C), and 1350 cm^{-1} for ν(C–OH), mainly owing to Lewis base interaction with Lewis acid of Pb^{2+} and Cs^+/FA^+/MA^+ ions.[24]

X-ray diffraction (XRD), scanning electron microscope (SEM), AFM and grazing incidence X-ray diffraction (GIXRD) measurements were utilized to investigate further the alteration of the perovskite film's crystal structure and morphological properties with and without Dec-oxoG NSs. The perovskite layer's XRD pattern (Figure 2b) showed predominant crystallization along the (001) plane that was consistent between the samples under investigation. Yet, both perovskites of the patterns have the peak relating to the intentionally used excess PbI_2 at $\approx$12.6°, although the perovskite film with Dec-oxoG NSs currently has more dominance.[25] This is attributed to that restructuring perovskite by Dec-oxoG NSs releases more PbI_2. Going further, we found that the Dec-oxoG-treated perovskite showed a reduced full width at half maximum (FWHM), corresponding to improved film crystallinity.

We subsequently elucidate the impact of the Dec-oxoG NSs on perovskite film morphology. As is depicted in the SEM images (Figure 2c,d), the perovskite film with Dec-oxoG NSs shows a more compact film with large crystals (Figure S4, ESI†), resulting in reduced grain boundaries where defects mainly exist.[26] Increased grain size generally benefits in light absorption and charge transfer in perovskite films.[27] The white crystals on the film surface indicate excessive/residual PbI_2 in previous reports.[28] Moreover, the root-mean-square surface roughness (R_{rms}) of the perovskite films is estimated from AFM images ($1\times1\ \mu m^2$) to be 10.5 nm after covering Dec-oxoG NSs onto perovskite film (Figure 2e,f) while that for reference perovskite film is 12.2 nm. The decreased R_{rms} is expected to improve the coverage of the electron transport layer.[7b]

To investigate the effect of Dec-oxoG NSs on perovskite structure, we performed grazing incidence wide-angle X-ray scattering (GIWAXS) measurements on the films. The one-dimensional (1D) GIWAXS patterns were integrated from corresponding 2D images. The estimated penetration depth with different incident angles was presented in Figure S5, ESI†. The introduction of Dec-oxoG NSs caused the scattering vector q peak within low incident angles to move to a smaller angle (Figure 3a,b). This indicates the extended lattice spacing due to the interaction between Dec-oxoG NSs and perovskites. This structural change is believed to lower the energy barrier at the perovskite-contact interface, thereby improving the open-circuit voltage (V_{oc}) and fill factor (FF) of solar cells.[29] As the incident angle increases (from 0.1° to 0.5°), the q's shift decreases (Figure 3b), suggesting that the structural effect mainly exists on the upper surface of the perovskite film. The initial weak diffraction intensity at low angles (0.1–0.2 degrees) originates from the highly defective Dec-oxoG NSs coverage. We observed a weak PbI_2 peak in the reference perovskite (Figure 3c). Strikingly, the PbI_2 phase in the Dec-oxoG NSs-treated perovskite increased gradually with the incidence angle (Figure 3d). Diffraction patterns at 2 degree were presented in Figure S6, ESI†, with the diffraction signal of labelled PbI_2 in the Dec-oxoG NSs based perovskite. The GIWAXS profile with the grazing incidence angle was presented in Figure S7, ESI†, which gave the signal evolution of PbI_2. These results indicate that the treatment of Dec-oxoG NSs allows additional PbI_2 to be released from perovskite by restructuring perovskites. Additionally, the faint peak located around 11.7° in Figure 3c corresponds to the hexagonal phase, which could be greatly suppressed by Dec-oxoG NSs (Figure 3d).[7] To further investigate the structural properties of perovskites influenced by Dec-oxoG NSs, we aged the unencapsulated films in air for one week. As a result, the reference perovskite film underwent degradation, manifested by enhanced PbI_2 content (Figure 3e) and increased grain boundaries (Figure S8a, ESI†). On the contrary, the morphology and structure of Dec-oxoG NSs treated perovskites are almost retained, exhibiting excellent film stability (Figures 3f and S8b, ESI†). Although more PbI_2 was detected in the new Dec-oxoG NSs-treated perovskites, PbI_2 content is not further increased, indicating that the perovskite retains structure stability during ageing.

Providing these results, we demonstrated that the Dec-oxoG NSs treatment effectively stabilized excess/unreacted PbI_2 left after the crystallization (Figure 3g,h). The excess PbI_2 at the grain boundaries is expelled to allow the smaller crystal to fuse to larger domains in an Ostwald ripening process.[26a,30] Also, the bound PbI_2 can prevent self-decomposition that induces perovskite degradation (Figure S9, ESI†).[13a,15a,31] The benefited perovskite stability is expected to enhance the operational durability of PV device.

Boosted charge carrier dynamics

For further understanding the impact of Dec-oxoG NSs on the charge recombination kinetics in the perovskite layers, we performed steady-state photoluminescence (PL), time-resolved photoluminescence (TRPL) and PL mapping. The maximum PL at the same wavelength for perovskite films were compared. Zhu et al. demonstrated that the improvement in PL intensity and carrier lifetime could be achieved by additive engineering. In their study, the –COOH-based ligand molecule altered the crystal growth of the perovskite layer and passivated defects from uncoordinated Pb^{2+}.[32] Similarly, Dec-oxoG NSs incorporated perovskite film presented stronger PL emission with a longer carrier lifetime

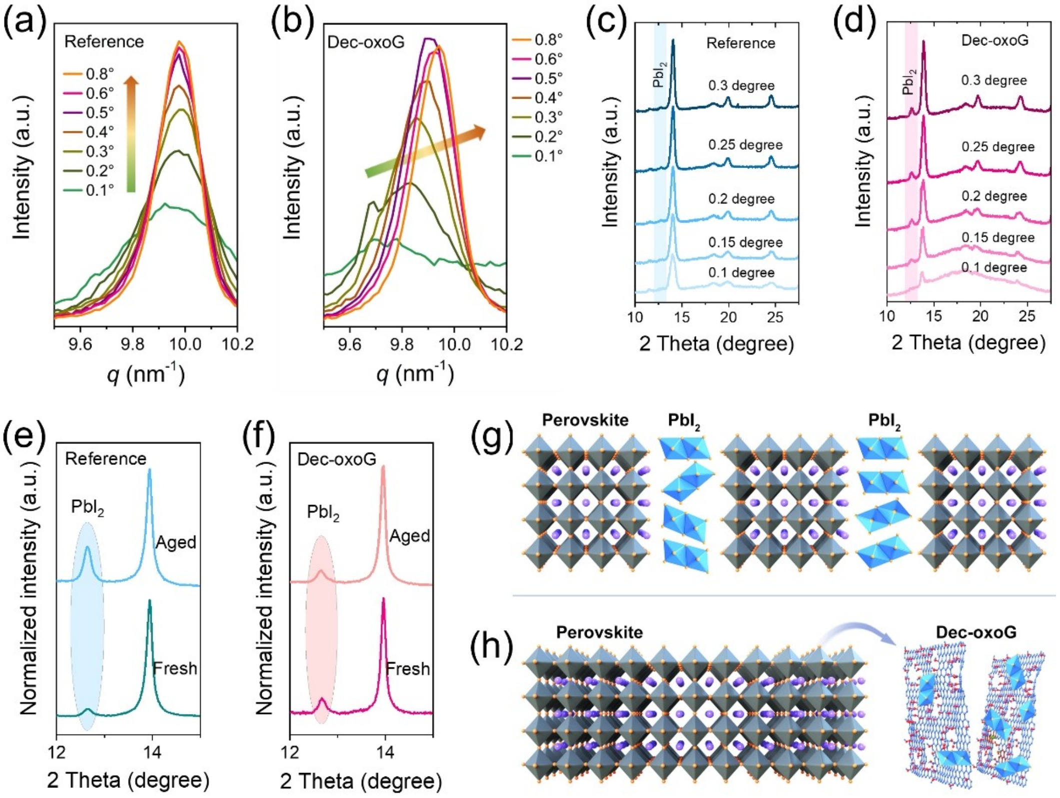

Figure 3. Integrated GIWAXS patterns on (001) peaks of (a) reference and (b) Dec-oxoG NSs perovskite films with incident 0.1 degree to 0.8 degree. Integrated GIWAXS patterns of (c) reference and (d) Dec-oxoG NSs perovskite films with incident 0.1 degree to 0.3 degree. XRD patterns of the (e) reference and (f) Dec-oxoG perovskite films undergoing ageing in the air for one week (ambient oxygen, 24 % humidity and light). Schematics of forming (g) reference and (h) Dec-oxoG perovskite films.

(over 3 μs) than reference perovskite film on the quartz, as indicated in Figures S10 and S11, as well as Table S1, ESI†. Enhanced PL intensity and carrier lifetime means the passivation effect of the -COOH-based Dec-oxoG NSs in perovskite film. The increased quasi-Fermi level splitting (QFLS) value also accounts for the reduced nonradiative recombination of carriers (Figure S12, ESI†). Figure 4a–d shows hyperspectral PL and QFLS maps measured at the exact location with a large-size area (around 2.2*2.2 cm^2) for typical samples with a stack of indium tin oxide (ITO) substrate/[2-(3,6-dimethoxy-9H-carbazol-9-yl)ethyl]phosphonic acid (MeO-2PACz)/perovskite. The excitation source is 455 nm LED, and the photon flux was 1.31 e^{21} (m^{-2}s^{-1}) under one sun condition. The reference sample has PL emission inhomogeneities on the bottom part of the substrate, which can be observed from PL peak and QFLS images. The Dec-oxoG NSs treated film shows a uniform emission distribution. Also, the Dec-oxoG NSs based film has higher PL intensity and QFLS values. It means that the Dec-oxoG NSs treatment doesn't only make the film more homogeneous but decreases the nonradiative recombination centers. We show that Dec-oxoG NSs can be successfully used for passivating film defects.

We subsequently investigated the charge carrier dynamics caused by Dec-oxoG NSs using the transient surface photovoltage (trSPV) measurements.[33] In Figure S13, ESI†, the panel describes charge separation mechanisms in the thin film of perovskite without transport layers. Dec-oxoG NSs treated perovskite film showed the increase in the negative SPV signal, indicating the dominance of free electrons near the top surface. The result for ITO/Pero/Dec-oxoG interface demonstrates that Dec-oxoG NSs boost the concertation of electrons near the perovskite surface due to the suppression of non-radiative recombination. We then studied the effect of Dec-oxoG NSs on charge extraction by constructing the device layer by layer and measuring trSPV. In Figure 4e, a self-assembled monolayer (SAM) of MeO–2PACz as a hole-selective contact (HSC) is incorporated between the ITO substrate and perovskite layer. Surprisingly, we found that Dec-oxoG NSs significantly boost the extraction rate of free holes, which is, to the best of your knowledge, the first observation of such a significant effect of a top layer on the bottom-hole extraction process. This effect is possibly induced by larger charge carrier mobility in Dec-oxoG NSs treated perovskite films due to better crystallinity, reduced trap concentration, and larger perovskite grains. This hypothesis is supported by photoluminescence maps showing much wider bright regions in Dec-oxoG NSs treated samples. Further, we deposited electron-selective contacts (ESC) on the perovskite surface to monitor the effect of Dec-oxoG NSs on interfacial electron extraction. As depicted in Figure 4f, the trSPV

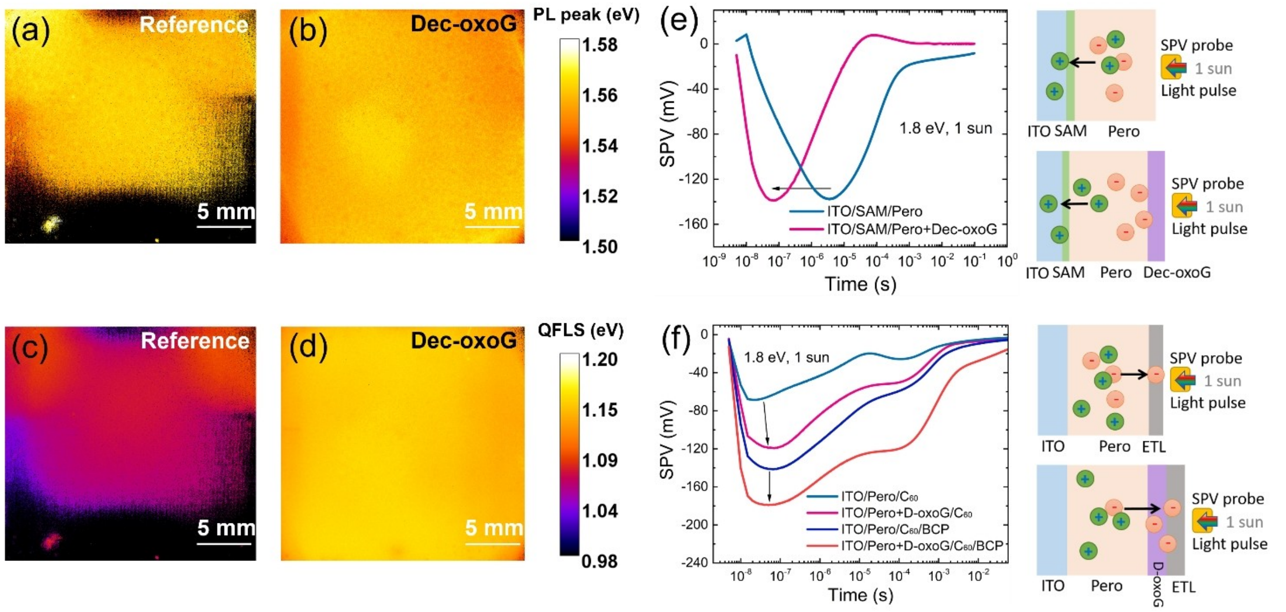

Figure 4. Photoluminescence maps of (a) reference and (b) Dec-oxoG perovskite films. Quasi-Fermi level splitting maps for (c) reference and (d) Dec-oxoG perovskite films. Imaging analysis measurements were prepared on the stack of glass/ITO/MeO-2PACz/perovskite. The excitation source is 455 nm LED, and the photon flux was $1.31\ e^{21}\ m^{-2}\ s^{-1}$ (one sun condition). Surface photovoltage transients of (e) ITO/MeO-2PACz/perovskite and (f) ITO/perovskite/C_{60} and ITO/perovskite/C_{60}/BCP, where both treated with Dec-oxoG NSs and untreated perovskites were studied. Schematic models representing photoexcitation by a nanosecond laser pulse, charge generation, and transport to ESC or HSC are provided on the right.

amplitude and signal rise time of ITO/perovskite with Dec-oxoG NSs/C_{60} sample are greater than that of ITO/perovskite/C_{60} sample. It suggests that Dec-oxoG NSs also boost electron extraction in the perovskite/C_{60} interface. The bathocuproine (BCP) layer further boosts electron extraction across the device (Figure 4f). The trSPV results are consistent in the visible spectrum range (1.5 to 3 eV). We also observed passivating capabilities of the Dec-oxoG NSs layer on perovskites (Figure S14, ESI[†]).

The insights into the mechanism of the charge carrier recombination process in PV devices are also investigated. The minimized nonradiative recombination losses in the device can be demonstrated from the dark current density-voltage (J–V) curves (Figure S15 and Table S2, ESI[†]), implying higher V_{oc} in the device.[34] Additionally, the increased resistance in Nyquist plots implicates better interfacial contact and favorable electron transfer at the perovskite/ETL interface for PSCs with Dec-oxoG NSs treatment (Figure S16, ESI[†]).[35] The increased build-in potential of Dec-oxoG NSs based device was verified from Mott–Schottky's analysis (Figure S17, ESI[†]), attributing to improving the V_{oc}.[36] The space-charge limited current (SCLC) model for electron-only devices was measured to understand the enhanced conductivity (Figure S18, ESI[†]). The reduced electron trap density could be attributed to the fact that Dec-oxoG NSs passivate the trap states (e.g., uncoordinated Pb^{2+}) by forming Lewis adducts.

Photovoltaic performance in p-i-n perovskite solar cells

The passivating effect of the Dec-oxoG NSs in the completed perovskite device performance is investigated by comparing with the reference device. The state-of-the-art device's architecture is based on the inverted p-i-n configuration of glass/ITO/MeO-2PACz/perovskite/C_{60}/BCP/silver (Ag), as shown in the cross-sectional SEM image (Figure 5a). Herein, the light absorber layer is passivated with Dec-oxoG NSs, and the thin thickness of these nanosheets prevents their detection. The device treated with 0.2 mg/mL Dec-oxoG NSs exhibited champion efficiency compared to concentration (Figure S19 and Table S3, ESI[†]). The uniform and pinhole-free perovskite film, after incorporating Dec-oxoG NSs, is worth noting that covers the MeO-2PACz molecule surface. Herein, the MeO-2PACz molecule was preferred as a hole-selective contact because its phosphonic acid anchoring group quickly formed a condensation reaction with the hydroxyl groups of the metal oxide by a spin-coating method.[37] The new device performance statistically surpassed an average of 20.5 % with the MeO-2PACz molecule in Figure 5b, in agreement with the literature work using the p-i-n architecture with triple-cation perovskite as an absorber.[37–38] Dec-oxoG NSs optimized device efficiency exceeds 22 % average. The best performance from the reference device exhibited a V_{oc} of 1.121 V, a FF of 81.5 %, a short-circuit current density (J_{sc}) of 24.1 mA/cm^2, and a PCE of 22.0 % (Figure 5c). In contrast, the device with modified Dec-oxoG NSs gave a V_{oc} of 1.147 V, a FF of 82.9 %, a J_{sc} of 24.3 mA/cm^2, and a PCE of 23.1 %. This boosting effect by

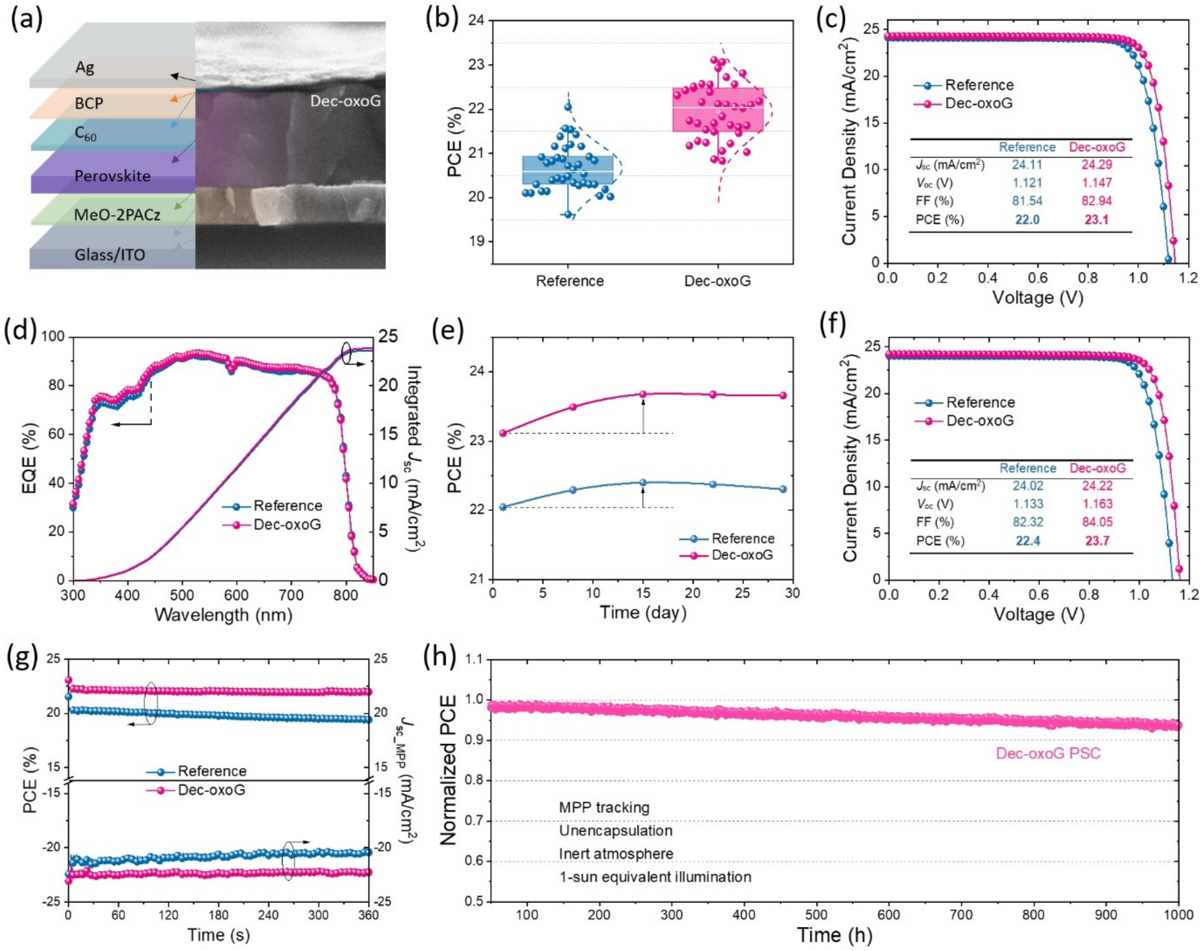

	Reference	Dec-oxoG
J_{sc} (mA/cm²)	24.11	24.29
V_{oc} (V)	1.121	1.147
FF (%)	81.54	82.94
PCE (%)	**22.0**	**23.1**

	Reference	Dec-oxoG
J_{sc} (mA/cm²)	24.02	24.22
V_{oc} (V)	1.133	1.163
FF (%)	82.32	84.05
PCE (%)	**22.4**	**23.7**

Figure 5. (a) Device architecture with cross-sectional SEM image of the PSCs. (b) The box charts of statistical PCEs from 19 devices that were performed forward sweep and reverse sweep, (c) the best-performing *J–V* curves and (d) EQE curves of new reference and Dec-oxoG-based PSCs. (e) Self-healing optimal device efficiency evolution and (f) champion *J–V* curves for reference and Dec-oxoG-based PSCs stored in the dark for one month. (g) The stabilized power outputs with MPP as a function of time. (h) The long-term stability of unencapsulated Dec-oxoG-based device under continuous MPP tracking in N_2 atmosphere. The data were normalized to the initial PCE value, presented after 50 h burning in.

Dec-oxoG NSs was also significantly greater than that of the oxoG-based device (Figure S20 and Table S4, ESI†). The *J–V* curves with the reverse and forward scans of the best-performing reference and Dec-oxoG NSs modified devices showed negligible hysteresis, respectively 1.8 % and 1.3 % (Figure S21 and Table S5, ESI†). As shown in the statistical distribution of box charts (Figure S22, ESI†), V_{oc} and FF parameters are significantly increased, thanks to the effective passivation of Dec-oxoG NSs. To passivate the ionic defects at the grain boundaries and interface of perovskite films are crucial for reaching high solar cell efficiency as discussed above.[15c,39] Figure 5d displays the external quantum efficiency (EQE) spectra for the champion PSCs. Integrated J_{sc} values present a negligible difference ($\approx$0.4 mA/cm²) with the J_{sc} values gained from the *J–V* scans. Subsequently, we monitored the PV performance evolution of devices stored in the dark for one month. As storage time increases to 15 days, we can observe a gradual increase in device efficiency (Figure 5e). The efficiency then showed relatively stable values from 15 to 28 days. In this process, the PCE of the control device increased to 22.4 %, having V_{oc} of 1.133 V, FF of 82.3 % and J_{sc} of 24.0 mA/cm² (Figure 5f). The Dec-oxoG NSs device delivered a remarkable PCE of 23.7 %, with an increased V_{oc} of 1.163 V, FF of 84.1 %, and a J_{sc} of 24.2 mA/cm². The reverse- and forward-scanned *J–V* curves are displayed in Figure S23 and Table S6, ESI†. The improved device performance under storage conditions is contributed by the introduction of Dec-oxoG NSs enhancing the self-healing ability of perovskite to minimize nonradiative recombination losses (Figures S24–S26, ESI†). Additionally, we measured the power outputs shown with photocurrent under maximum power points (MPP) tracking. As shown in Figure 5g, the Dec-oxoG PSCs possessed a more stable power output than reference PSCs, showing higher photostability (Figures S27, ESI†). For this reason, we further measured the long-term stability under continuous one-sun illumination at MPP for Dec-oxoG-based PSCs to certify the reliability. As shown in Figure 5h, the Dec-oxoG-based device retained 93.8 % efficiency after 1,000 h tracking, reflecting a significant device stability by

Dec-oxoG NSs optimization. In addition, the thermal stability of the device that tested at 85 °C is also well improved (Figure S28, ESI†). The solar cell also shows enhanced stability under ambient condition, exposing to oxygen and humidity of air (Figure S29, ESI†). The improved efficiency of PSCs is attributed to the Dec-oxoG NSs-optimized perovskite film quality, and further managing PbI_2 enhances the device's operational stability. This work's resultant PV performance (PCEs and stability) is superior to those previously reported that applied low dimensional (2D) materials, such as MXene,[40] black phosphorous,[41] boron nitrides,[42] transitional metal dichalcogenides,[43] and graphene and its derivatives,[44] to improve PSCs' stability or efficiency.

Conclusion

Functional two-dimensional materials can meet specific needs by introducing functional groups for multi-functionalization. As the Dec-oxoG NSs we designed in this work, defect passivation and crystal stabilization are achieved simultaneously. Perovskite films and integrated devices with Dec-oxoG NSs modulation show reduced defect density, facilitated electron and hole transfer, and enhanced structural stability. We propose a mechanism of Dec-oxoG NSs in strengthening and stabilizing PSCs performance: (i) introducing Dec-oxoG NSs triggers Ostwald ripening, leading to grain-enlarged and flatter perovskite films, releasing additional PbI_2 to be captured by Dec-oxoG NSs (managing PbI_2 to fabricate high-quality perovskites); (ii) Dec-oxoG NSs prevents the degradation of perovskite polycrystalline and even the further generation of PbI_2 from films (stabilizing perovskites); (iii) Dec-oxoG NSs stabilize residual PbI_2 with solid bonds and then reduce perovskite crystal structure damage (preventing PbI_2 damage to perovskites).

As a proof of concept, by employing functional-rich Dec-oxoG NSs to passivate and stabilize the perovskite structure, we reported a PCE of up to 23.7 % in p-i-n PSCs. Furthermore, the Dec-oxoG-based PSC showed excellent operational stability, which retained 93.8 % of its initial efficiency with MPP tracking under continuous one sun illumination exceeding 1,000 hours. The optimized solar cells also exhibited high stabilities in elevated temperature and ambient conditions. This work provides an approach to design functionalized ultra-thin 2D materials for efficient photostability of PSCs but also shows a novel perspective on stabilizing perovskite crystals by manipulating PbI_2 for photovoltaic, electronic devices, taking into account the advantages of excess PbI_2 for fabricating high-quality perovskite films.

Acknowledgements

We thank Helmholtz-Zentrum Berlin (HZB) for funding and technical support. G.L., J.L., S.Z. and K.P. thank the support from the HyPerCells Joint Graduate School at HZB. Thanks to Dr. Janardan Dagar for assisting in AFM measurements. HySPRINT Helmholtz Innovation Lab that provides the infrastructure and Prof. Dr. Steve Albrecht's team for lab setup support are acknowledged. K.P. acknowledges the Deutscher Akademischer Austauschdienst (DAAD) for funding via the Research Grants - Doctoral Programmes in Germany, 2018/19 (57381412). B.A.-T. appreciates the support from the TWAS-DFG Programme. The authors gratefully acknowledge the facility of the HZB SPV lab led by Thomas Dittrich. The authors thank mySpot (BESSY II, HZB, Germany) for providing the synchrotron radiation beamtime. The authors acknowledge Park Systems for support. This project has received funding from the European Union's Framework Programme for Research and Innovation HORIZON EUROPE (2021–2027) under the Marie Skłodowska-Curie Action Postdoctoral Fellowships (European Fellowship) 101061809 HyPerGreen. This work has received funding from the European Research Council (ERC) under the European Union's Horizon 2020 research and innovation programme (Grant agreement No. 804519). Open Access funding enabled and organized by Projekt DEAL.

Conflict of Interest

The authors declare no conflict of interest.

Data Availability Statement

Research data are not shared.

Keywords: Excess Lead Iodide · Operational Stability · Oxo-Graphene Nanosheets · Perovskite Photovoltaics · Solar Cells

[1] a) A. Kojima, K. Teshima, Y. Shirai, T. Miyasaka, *J. Am. Chem. Soc.* **2009**, *131*, 6050–6051; b) NREL, Best Research-Cell Efficiency Chart, https://www.nrel.gov/pv/cell-efficiency.html **2023**.

[2] P. C. Harikesh, B. Wu, B. Ghosh, R. A. John, S. Lie, K. Thirumal, L. H. Wong, T. C. Sum, S. Mhaisalkar, N. Mathews, *Adv. Mater.* **2018**, *30*, 1802080.

[3] G. E. Eperon, S. D. Stranks, C. Menelaou, M. B. Johnston, L. M. Herz, H. J. Snaith, *Energy Environ. Sci.* **2014**, *7*, 982–988.

[4] G.-W. Kim, A. Petrozza, *Adv. Energy Mater.* **2020**, *10*, 2001959.

[5] Z. Yang, Z. Yu, H. Wei, X. Xiao, Z. Ni, B. Chen, Y. Deng, S. N. Habisreutinger, X. Chen, K. Wang, J. Zhao, P. N. Rudd, J. J. Berry, M. C. Beard, J. Huang, *Nat. Commun.* **2019**, *10*, 4498.

[6] L. Chouhan, S. Ghimire, C. Subrahmanyam, T. Miyasaka, V. Biju, *Chem. Soc. Rev.* **2020**, *49*, 2869–2885.

[7] a) G. Li, Z. Su, M. Li, H. K. H. Lee, R. Datt, D. Hughes, C. Wang, M. Flatken, H. Köbler, J. J. Jerónimo-Rendon, R. Roy, F. Yang, J. Pascual, Z. Li, W. C. Tsoi, X. Gao, Z. Wang, M. Saliba, A. Abate, *Adv. Energy Mater.* **2022**, *12*, 2202887; b) G. Li, Z. Su, L. Canil, D. Hughes, M. H. Aldamasy, J. Dagar, S. Trofimov, L. Wang, W. Zuo, J. J. Jerónimo-Rendon, M. M. Byranvand, C. Wang, R. Zhu, Z. Zhang, F. Yang, G. Nasti, B.

Naydenov, W. C. Tsoi, Z. Li, X. Gao, Z. Wang, Y. Jia, E. Unger, M. Saliba, M. Li, A. Abate, *Science* **2023**, *379*, 399–403.

[8] M. Saliba, T. Matsui, J.-Y. Seo, K. Domanski, J.-P. Correa-Baena, M. K. Nazeeruddin, S. M. Zakeeruddin, W. Tress, A. Abate, A. Hagfeldt, M. Grätzel, *Energy Environ. Sci.* **2016**, *9*, 1989–1997.

[9] a) A. Farooq, M. R. Khan, T. Abzieher, A. Voigt, D. C. Lupascu, U. Lemmer, B. S. Richards, U. W. Paetzold, *ACS Appl. Energ. Mater.* **2021**, *4*, 3083–3092; b) M. Saliba, J.-P. Correa-Baena, C. M. Wolff, M. Stolterfoht, N. Phung, S. Albrecht, D. Neher, A. Abate, *Chem. Mater.* **2018**, *30*, 4193–4201; c) M. Saliba, T. Matsui, K. Domanski, J.-Y. Seo, A. Ummadisingu, S. M. Zakeeruddin, J.-P. Correa-Baena, W. R. Tress, A. Abate, A. Hagfeldt, M. Grätzel, *Science* **2016**, *354*, 206–209.

[10] a) C. Yi, J. Luo, S. Meloni, A. Boziki, N. Ashari-Astani, C. Grätzel, S. M. Zakeeruddin, U. Röthlisberger, M. Grätzel, *Energy Environ. Sci.* **2016**, *9*, 656–662; b) Z. Li, M. Yang, J.-S. Park, S.-H. Wei, J. J. Berry, K. Zhu, *Chem. Mater.* **2016**, *28*, 284–292.

[11] a) K. Domanski, B. Roose, T. Matsui, M. Saliba, S.-H. Turren-Cruz, J.-P. Correa-Baena, C. R. Carmona, G. Richardson, J. M. Foster, F. De Angelis, J. M. Ball, A. Petrozza, N. Mine, M. K. Nazeeruddin, W. Tress, M. Grätzel, U. Steiner, A. Hagfeldt, A. Abate, *Energy Environ. Sci.* **2017**, *10*, 604–613; b) A. Gomez, S. Sanchez, M. Campoy-Quiles, A. Abate, *Nano Energy* **2018**, *45*, 94–100.

[12] a) E. T. Hoke, D. J. Slotcavage, E. R. Dohner, A. R. Bowring, H. I. Karunadasa, M. D. McGehee, *Chem. Sci.* **2015**, *6*, 613–617; b) L. McGovern, G. Grimaldi, M. H. Futscher, E. M. Hutter, L. A. Muscarella, M. C. Schmidt, B. Ehrler, *ACS Appl. Energ. Mater.* **2021**, *4*, 13431–13437.

[13] a) L. Zhao, Q. Li, C.-H. Hou, S. Li, X. Yang, J. Wu, S. Zhang, Q. Hu, Y. Wang, Y. Zhang, Y. Jiang, S. Jia, J.-J. Shyue, T. P. Russell, Q. Gong, X. Hu, R. Zhu, *J. Am. Chem. Soc.* **2022**, *144*, 1700–1708; b) B.-w. Park, N. Kedem, M. Kulbak, D. Y. Lee, W. S. Yang, N. J. Jeon, J. Seo, G. Kim, K. J. Kim, T. J. Shin, G. Hodes, D. Cahen, S. I. Seok, *Nat. Commun.* **2018**, *9*, 3301; c) T. J. Jacobsson, J.-P. Correa-Baena, E. Halvani Anaraki, B. Philippe, S. D. Stranks, M. E. F. Bouduban, W. Tress, K. Schenk, J. Teuscher, J.-E. Moser, H. Rensmo, A. Hagfeldt, *J. Am. Chem. Soc.* **2016**, *138*, 10331–10343.

[14] Q. Jiang, Z. Chu, P. Wang, X. Yang, H. Liu, Y. Wang, Z. Yin, J. Wu, X. Zhang, J. You, *Adv. Mater.* **2017**, *29*, 1703852.

[15] a) J. Liang, X. Hu, C. Wang, C. Liang, C. Chen, M. Xiao, J. Li, C. Tao, G. Xing, R. Yu, W. Ke, G. Fang, *Joule* **2022**, *6*, 816–833; b) S. Wang, Y. Jiang, E. J. Juarez-Perez, L. K. Ono, Y. Qi, *Nat. Energy* **2016**, *2*, 16195; c) L. Fu, H. Li, L. Wang, R. Yin, B. Li, L. Yin, *Energy Environ. Sci.* **2020**, *13*, 4017–4056.

[16] a) B. Wang, J. Iocozzia, M. Zhang, M. Ye, S. Yan, H. Jin, S. Wang, Z. Zou, Z. Lin, *Chem. Soc. Rev.* **2019**, *48*, 4854–4891; b) T. Mahmoudi, M. Kohan, W.-Y. Rho, Y. Wang, Y. H. Im, Y.-B. Hahn, *Adv. Energy Mater.* **2022**, *12*, 2201977; c) H. Chen, Y. Hou, C. E. Halbig, S. Chen, H. Zhang, N. Li, F. Guo, X. Tang, N. Gasparini, I. Levchuk, S. Kahmann, C. O. Ramirez Quiroz, A. Osvet, S. Eigler, C. J. Brabec, *J. Mater. Chem. A* **2016**, *4*, 11604–11610; d) B. Agyei-Tuffour, K. Mensah-Darkwa, D. N. Ampong, E. A. Addae, G. S. Gbadam, C. N. S. Darko, A. O. Akyaw, J. Adjah, J. Asare, G. Li, N. J. Goosen, *Cogent Eng.* **2022**, *9*, 2143034.

[17] X. Lin, H. Su, S. He, Y. Song, Y. Wang, Z. Qin, Y. Wu, X. Yang, Q. Han, J. Fang, Y. Zhang, H. Segawa, M. Grätzel, L. Han, *Nat. Energy* **2022**, *7*, 520–527.

[18] M. Li, W.-W. Zuo, Q. Wang, K.-L. Wang, M.-P. Zhuo, H. Köbler, C. E. Halbig, S. Eigler, Y.-G. Yang, X.-Y. Gao, Z.-K. Wang, Y. Li, A. Abate, *Adv. Energy Mater.* **2020**, *10*, 1902653.

[19] S. Eigler, M. Enzelberger-Heim, S. Grimm, P. Hofmann, W. Kroener, A. Geworski, C. Dotzer, M. Röckert, J. Xiao, C. Papp, O. Lytken, H.-P. Steinrück, P. Müller, A. Hirsch, *Adv. Mater.* **2013**, *25*, 3583–3587.

[20] Y. Hu, Q. Cao, C. Neumann, T. Lehnert, F. Börrnert, Y. Wang, U. Kaiser, A. Turchanin, S. Eigler, *Carbon* **2021**, *185*, 568–577.

[21] S. Eigler, C. Dotzer, F. Hof, W. Bauer, A. Hirsch, *Chem. Eur. J.* **2013**, *19*, 9490–9496.

[22] A. Lerf, H. He, M. Forster, J. Klinowski, *J. Phys. Chem. B* **1998**, *102*, 4477–4482.

[23] N. Ahn, D.-Y. Son, I.-H. Jang, S. M. Kang, M. Choi, N.-G. Park, *J. Am. Chem. Soc.* **2015**, *137*, 8696–8699.

[24] X. Guo, C. McCleese, W. Gao, M. Wang, L. Sang, C. Burda, *Mater. Renewable Sustainable Energy* **2016**, *5*, 17.

[25] B. Roose, K. Dey, Y.-H. Chiang, R. H. Friend, S. D. Stranks, *J. Phys. Chem. Lett.* **2020**, *11*, 6505–6512.

[26] a) N. D. Pham, V. T. Tiong, D. Yao, W. Martens, A. Guerrero, J. Bisquert, H. Wang, *Nano Energy* **2017**, *41*, 476–487; b) M. M. Tavakoli, M. Saliba, P. Yadav, P. Holzhey, A. Hagfeldt, S. M. Zakeeruddin, M. Grätzel, *Adv. Energy Mater.* **2019**, *9*, 1802646.

[27] a) G. Xing, N. Mathews, S. Sun, S. S. Lim, Y. M. Lam, M. Grätzel, S. Mhaisalkar, T. C. Sum, *Science* **2013**, *342*, 344–347; b) Q. Zhao, G. R. Li, J. Song, Y. Zhao, Y. Qiang, X. P. Gao, *Sci. Rep.* **2016**, *6*, 38670.

[28] a) Z. Hu, Q. An, H. Xiang, L. Aigouy, B. Sun, Y. Vaynzof, Z. Chen, *ACS Appl. Mater. Interfaces* **2020**, *12*, 54824–54832; b) B. Yang, J. Suo, E. Mosconi, D. Ricciarelli, W. Tress, F. De Angelis, H.-S. Kim, A. Hagfeldt, *ACS Energy Lett.* **2020**, *5*, 3159–3167.

[29] H. Tsai, R. Asadpour, J.-C. Blancon, C. C. Stoumpos, O. Durand, J. W. Strzalka, B. Chen, R. Verduzco, P. M. Ajayan, S. Tretiak, J. Even, M. A. Alam, M. G. Kanatzidis, W. Nie, A. D. Mohite, *Science* **2018**, *360*, 67–70.

[30] a) N. Li, X. Niu, L. Li, H. Wang, Z. Huang, Y. Zhang, Y. Chen, X. Zhang, C. Zhu, H. Zai, Y. Bai, S. Ma, H. Liu, X. Liu, Z. Guo, G. Liu, R. Fan, H. Chen, J. Wang, Y. Lun, X. Wang, J. Hong, H. Xie, D. S. Jakob, X. G. Xu, Q. Chen, H. Zhou, *Science* **2021**, *373*, 561–567; b) Y. Yang, J. Wu, X. Wang, Q. Guo, X. Liu, W. Sun, Y. Wei, Y. Huang, Z. Lan, M. Huang, J. Lin, H. Chen, Z. Wei, *Adv. Mater.* **2020**, *32*, 1904347.

[31] S. Macpherson, T. A. S. Doherty, A. J. Winchester, S. Kosar, D. N. Johnstone, Y.-H. Chiang, K. Galkowski, M. Anaya, K. Frohna, A. N. Iqbal, S. Nagane, B. Roose, Z. Andaji-Garmaroudi, K. W. P. Orr, J. E. Parker, P. A. Midgley, K. M. Dani, S. D. Stranks, *Nature* **2022**, *607*, 294–300.

[32] L. Zhu, X. Zhang, M. Li, X. Shang, K. Lei, B. Zhang, C. Chen, S. Zheng, H. Song, J. Chen, *Adv. Energy Mater.* **2021**, *11*, 2100529.

[33] I. Levine, A. Al-Ashouri, A. Musiienko, H. Hempel, A. Magomedov, A. Drevilkauskaite, V. Getautis, D. Menzel, K. Hinrichs, T. Unold, S. Albrecht, T. Dittrich, *Joule* **2021**, *5*, 2915–2933.

[34] C. M. Wolff, F. Zu, A. Paulke, L. P. Toro, N. Koch, D. Neher, *Adv. Mater.* **2017**, *29*, 1700159.

[35] J.-F. Wang, L. Zhu, B.-G. Zhao, Y.-L. Zhao, J. Song, X.-Q. Gu, Y.-H. Qiang, *Sci. Rep.* **2017**, *7*, 14478.

[36] Y. Wu, Q. Wang, Y. Chen, W. Qiu, Q. Peng, *Energy Environ. Sci.* **2022**, *15*, 4700–4709.

[37] A. Al-Ashouri, A. Magomedov, M. Roß, M. Jošt, M. Talaikis, G. Chistiakova, T. Bertram, J. A. Márquez, E. Köhnen, E. Kasparavičius, S. Levcenco, L. Gil-Escrig, C. J. Hages, R. Schlatmann, B. Rech, T. Malinauskas, T. Unold, C. A. Kaufmann, L. Korte, G. Niaura, V. Getautis, S. Albrecht, *Energy Environ. Sci.* **2019**, *12*, 3356–3369.

[38] N. Phung, M. Verheijen, A. Todinova, K. Datta, M. Verhage, A. Al-Ashouri, H. Köbler, X. Li, A. Abate, S. Albrecht, M. Creatore, *ACS Appl. Mater. Interfaces* **2022**, *14*, 2166–2176.

[39] a) X. Zheng, B. Chen, J. Dai, Y. Fang, Y. Bai, Y. Lin, H. Wei, X. C. Zeng, J. Huang, *Nat. Energy* **2017**, *2*, 17102; b) A. R. b Mohd Yusoff, M. Vasilopoulou, D. G. Georgiadou, L. C. Palilis, A. Abate, M. K. Nazeeruddin, *Energy Environ. Sci.* **2021**, *14*, 2906–2953.

[40] D. Saranin, S. Pescetelli, A. Pazniak, D. Rossi, A. Liedl, A. Yakusheva, L. Luchnikov, D. Podgorny, P. Gostischev, S. Didenko, A. Tameev, D. Lizzit, M. Angelucci, R. Cimino, R. Larciprete, A. Agresti, A. Di Carlo, *Nano Energy* **2021**, *82*, 105771.

[41] J. He, F. Zhang, Y. Xiang, J. Lian, X. Wang, Y. Zhang, X. Peng, P. Zeng, J. Qu, J. Song, *J. Power Sources* **2019**, *435*, 226819.

[42] D. S. Mann, P. Patil, D.-H. Kim, S.-N. Kwon, S.-I. Na, *J. Power Sources* **2020**, *477*, 228738.

[43] N. H. Hemasiri, S. Kazim, S. Ahmad, *Nano Energy* **2020**, *77*, 105292.

[44] a) Y. Yao, C. Cheng, C. Zhang, H. Hu, K. Wang, S. De Wolf, *Adv. Mater.* **2022**, *34*, 2203794; b) F. Ye, S. Zhang, J. Warby, J. Wu, E. Gutierrez-Partida, F. Lang, S. Shah, E. Saglamkaya, B. Sun, F. Zu, S. Shoaee, H. Wang, B. Stiller, D. Neher, W.-H. Zhu, M. Stolterfoht, Y. Wu, *Nat. Commun.* **2022**, *13*, 7454.

Manuscript received: May 25, 2023
Accepted manuscript online: July 31, 2023
Version of record online: ■■, ■■

Research Articles

Solar Cells

G. Li, Y. Hu, M. Li,* Y. Tang, Z. Zhang, A. Musiienko, Q. Cao, F. Akhundova, J. Li, K. Prashanthan, F. Yang, P. Janasik, A. N. S. Appiah, S. Trofimov, N. Livakas, S. Zuo, L. Wu, L. Wang, Y. Yang, B. Agyei-Tuffour, R. W. MacQueen, B. Naydenov, T. Unold, E. Unger, E. Aktas,* S. Eigler,* A. Abate* ——— **e202307395**

Managing Excess Lead Iodide with Functionalized Oxo-Graphene Nanosheets for Stable Perovskite Solar Cells

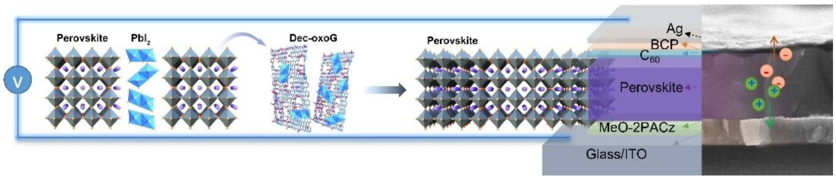

Effectively managing excess lead iodide is crucial for enhancing perovskite stability. An innovative approach, tailoring functionalized oxo-graphene nanosheets, stabilizes the perovskite structure and improves charge extraction. This leads to a significant boost in power conversion efficiency and long-term stability in inverted (p-i-n) perovskite solar cells, providing a novel perspective on stabilizing photovoltaic devices.